Supplementary Materials

Robust double-lock MXene anodes for stable sodium storage

Xuan Huang[1,2], Jiaqi Fei[1], Lingxia Fan[2], Lize Zhang[2], Xinghui Sun[2], Junfan Zhang[2], Chunguang Wei[2], Hongwei Bi[2,*], Aruuhan Bayaguud[1,*], Yelong Zhang[2,*]

[1]School of Materials Science and Engineering, Inner Mongolia University of Technology, Hohhot 010051, Inner Mongolia, China.
[2]School of New Energy, Inner Mongolia University of Technology, Ordos 017010, Inner Mongolia, China.

Correspondence to: Dr. Hongwei Bi, Prof. Yelong Zhang, School of New Energy, Inner Mongolia University of Technology, Ordos 017010, Inner Mongolia, China. E-mail: bhw@imut.edu.cn; ylzhang@imut.edu.cn; Prof. Aruuhan Bayaguud, School of Materials Science and Engineering, Inner Mongolia University of Technology, Hohhot 010051, Inner Mongolia, China. E-mail: jinaruhan@imut.edu.cn

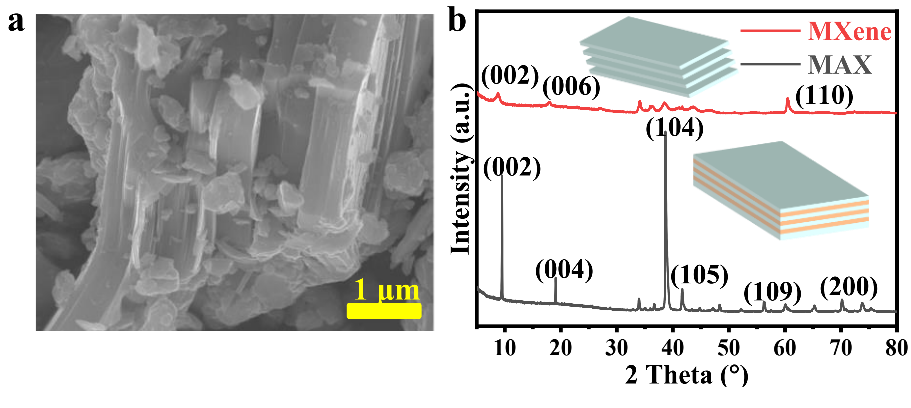

Supplementary Figure 1. a) SEM image of the precursor MAX phase. b) XRD pattern of the as-prepared Ti_3C_2.

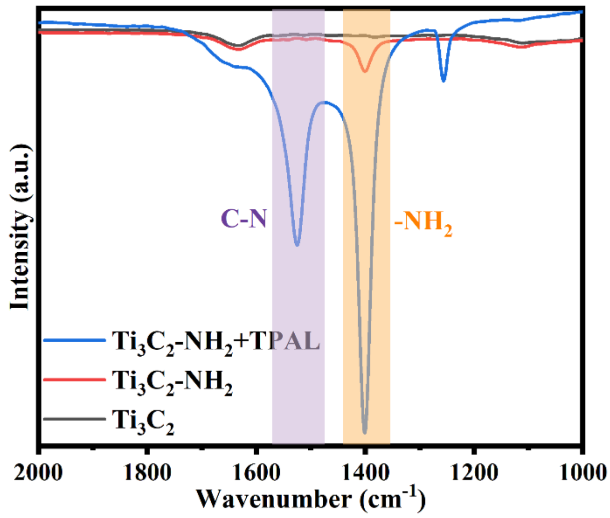

Supplementary Figure 2. FTIR spectra of Ti_3C_2, Ti_3C_2-NH_2, and the Ti_3C_2-NH_2+TPAL physical mixture. The physical mixture was prepared by mechanically mixing Ti_3C_2-NH_2 and TPAL.

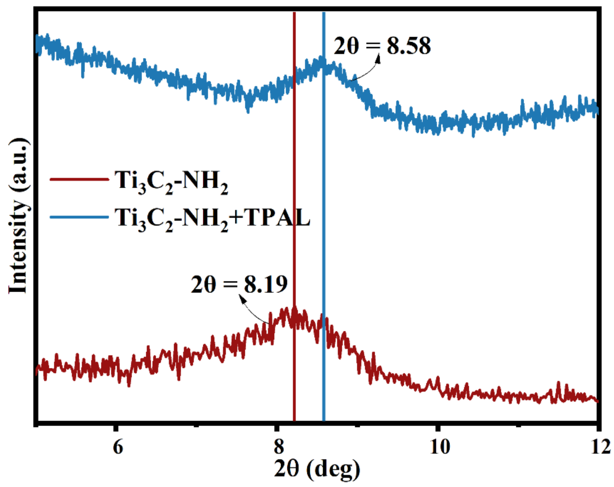

Supplementary Figure 3. FTIR spectra of Ti_3C_2-NH_2, and the Ti_3C_2-NH_2+TPAL physical mixture.

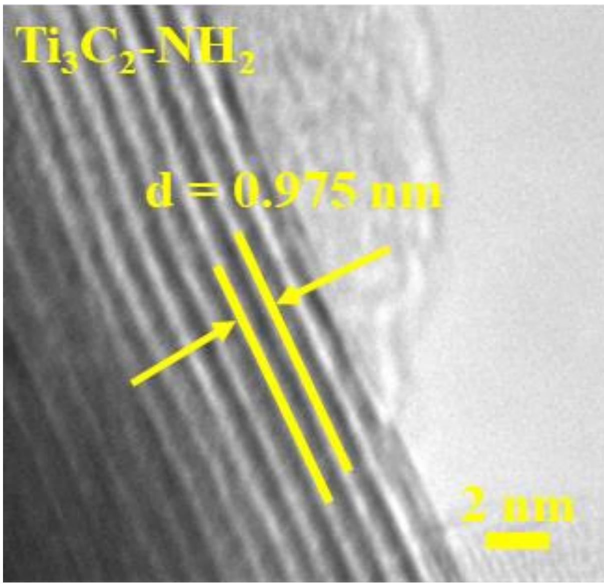

Supplementary Figure 4. HRTEM images of Ti_3C_2-NH_2

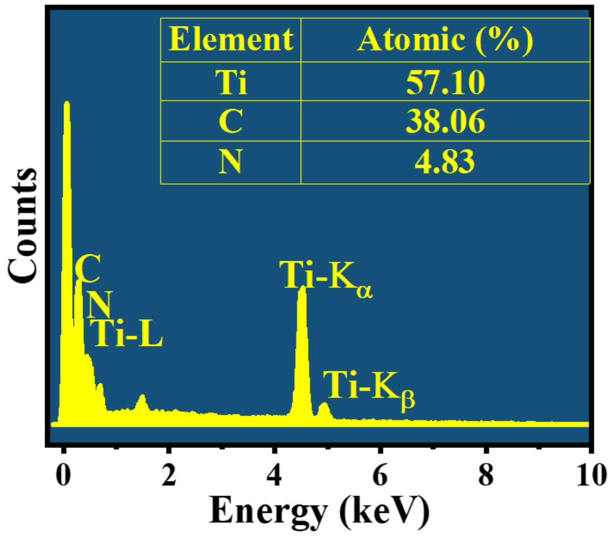

Supplementary Figure 5. EDX elemental analysis spectrum of Ti_3C_2-TPAL.

Note: Based on the atomic percentages of Ti (57.1 at%), C (38.06 at%), and N (4.83 at%), the mass fraction of grafted TPAL was estimated. Nitrogen serves as the specific marker for the grafted organic phase. The assumption is a 1:1 stoichiometry between nitrogen atoms and attached TPAL molecules derived from the Schiff base reaction. Using the atomic mass of N (14.01 g mol^{-1}), the relative mass of the grafted component corresponds to the nitrogen content converted via the molecular weight of TPAL (134.14 g mol^{-1}).

The Ti and C data are used to define the inorganic matrix mass, noting that the 3:2 Ti/C ratio aligns with Ti_3C_2 stoichiometry. The mass fraction is calculated by dividing the TPAL contribution by the total system mass (matrix plus graft). The results show that TPAL comprises approximately 16.9 wt% of the composite.

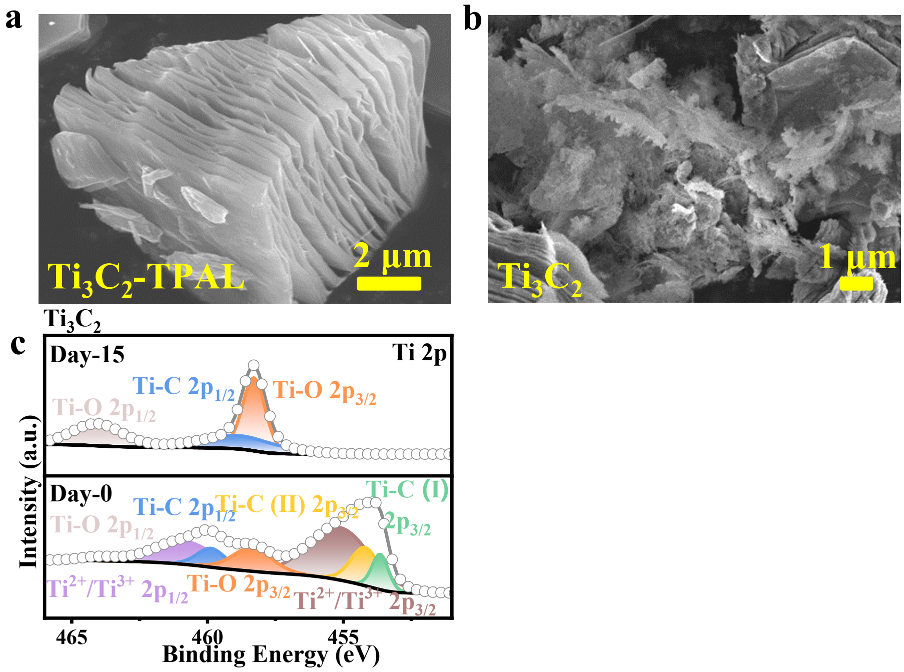

Supplementary Figure 6. SEM images of a) Ti_3C_2-TPAL and b) Ti_3C_2 after 15 days in air. c) High-resolution Ti 2p XPS spectra of Ti_3C_2 before and after air exposure.

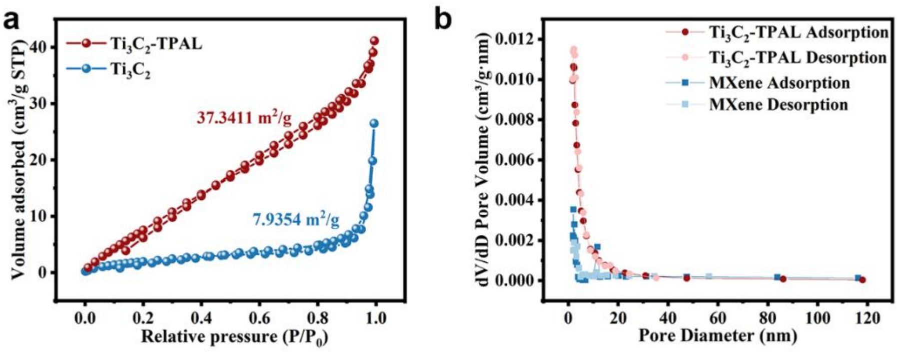

Supplementary Figure 7. N_2 adsorption-desorption isotherms and corresponding pore-size distributions of pristine Ti_3C_2 and Ti_3C_2-TPAL.

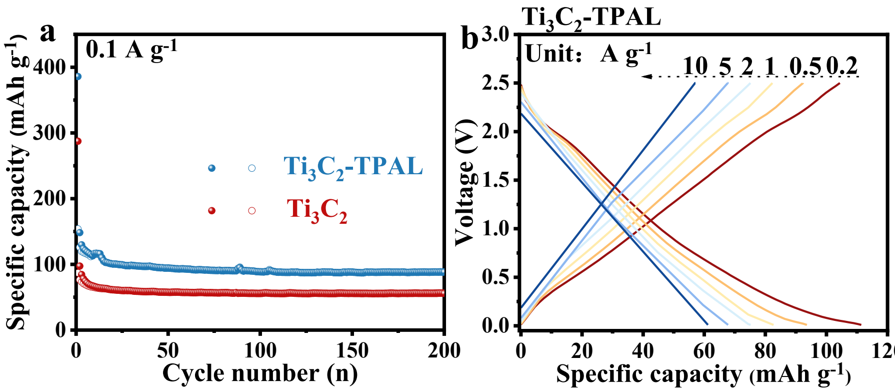

Supplementary Figure 8. a) Cycling performance at 0.1 Ag^{-1} and b) GCD curves at different current densities for Ti_3C_2-TPAL.

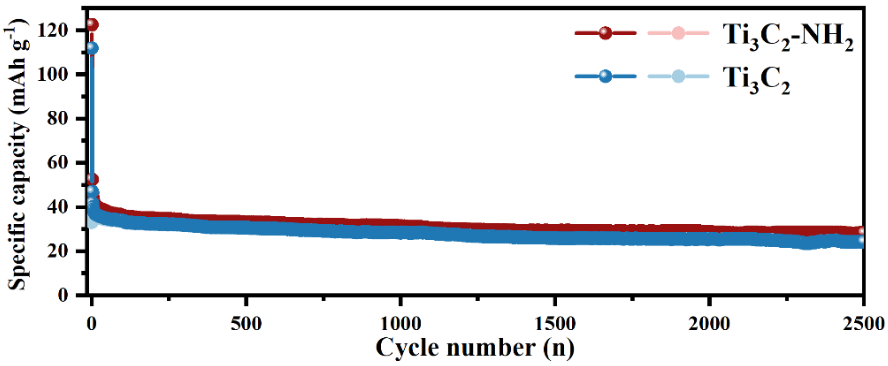

Supplementary Figure 9. a) Cycling performance of Ti_3C_2 and Ti_3C_2-NH_2 at 5 A g^{-1}.

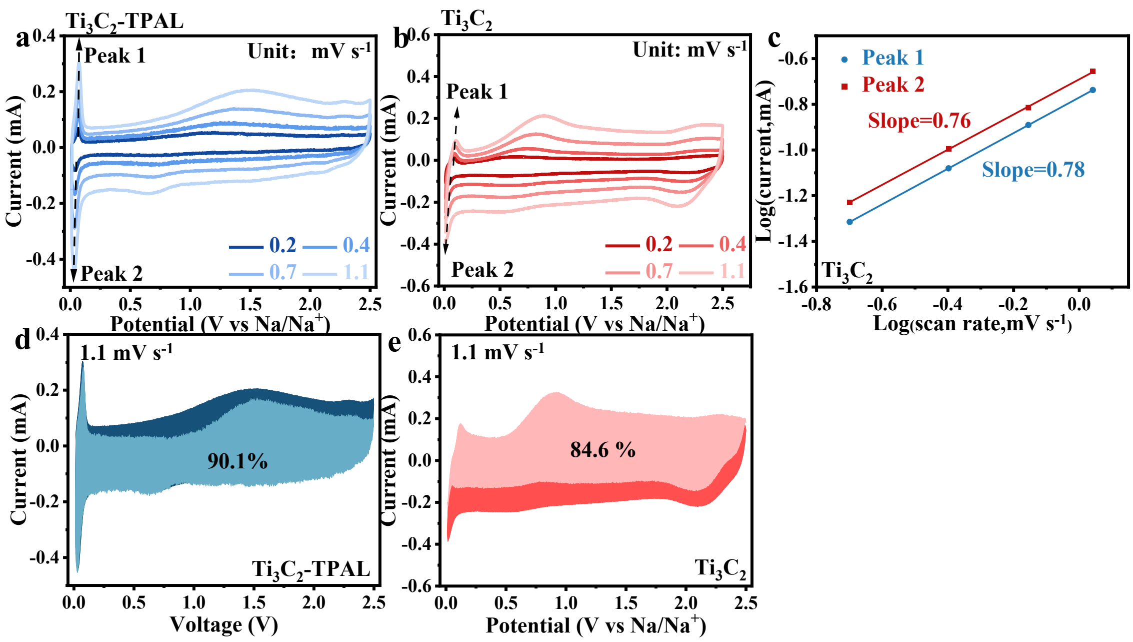

Supplementary Figure 10. CV curves of a) Ti_3C_2-TPAL and b) Ti_3C_2 measured at 0.2–1.1 mV s^{-1}. The corresponding log(i) versus log(v) plots for c) Ti_3C_2. Capacitive contribution ratios at 1.1 mV s^{-1} for d) Ti_3C_2-TPAL and e) Ti_3C_2.

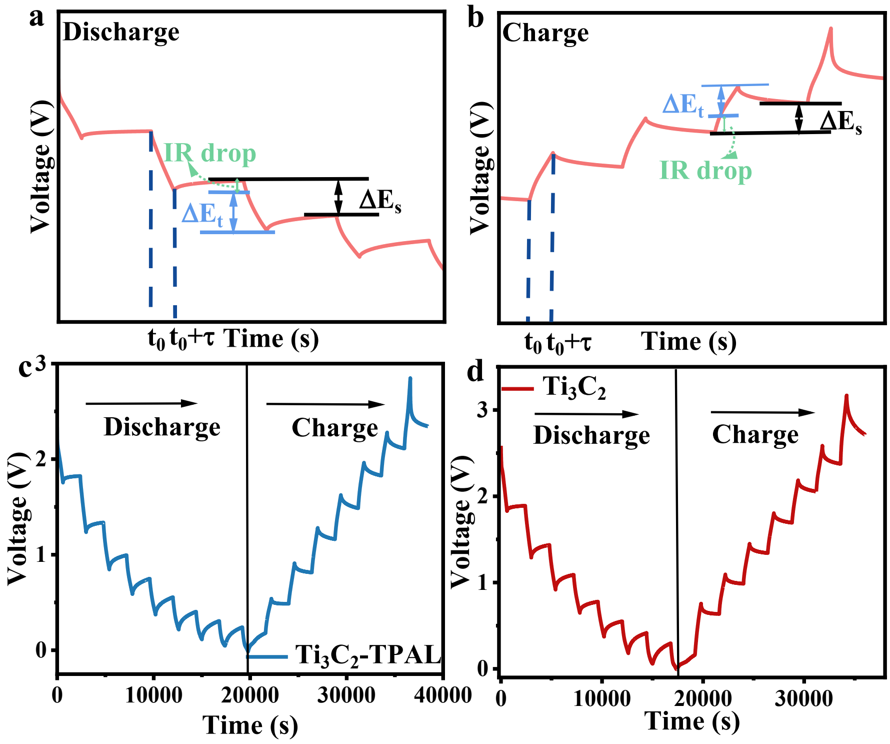

Supplementary Figure 11. Schematic illustrations of the GITT profiles during a) discharge and b) charge processes. GITT curves for c) Ti_3C_2-TPAL and d) Ti_3C_2.

Note: Note: Based on Fick's second law, the diffusion coefficient (D) was derived from GITT measurements using Equation (1).

$$D = \frac{4}{\pi\tau}\left(\frac{m_a V_M}{M_a S}\right)^2 \left(\frac{\Delta E_S}{\Delta E_\tau}\right)^2 \tag{1}$$

In this equation, τ is the current pulse duration; m_a and M_a are the active mass and molar mass of the material, respectively. V_M is the molar volume obtained from the density, and S is the electrode area. The terms ΔE_S and $\Delta E\tau$ represent the steady-state and transient voltage changes extracted from the GITT data.

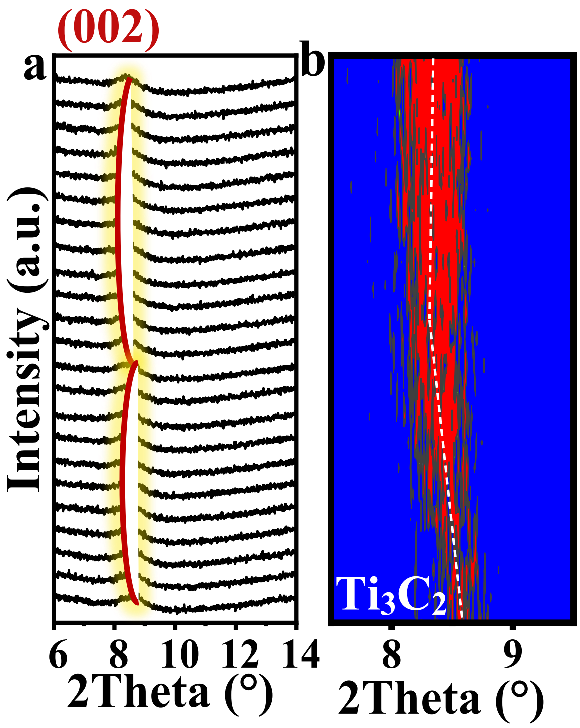

Supplementary Figure 12. *In-situ* XRD patterns of Ti_3C_2 during charge-discharge process.

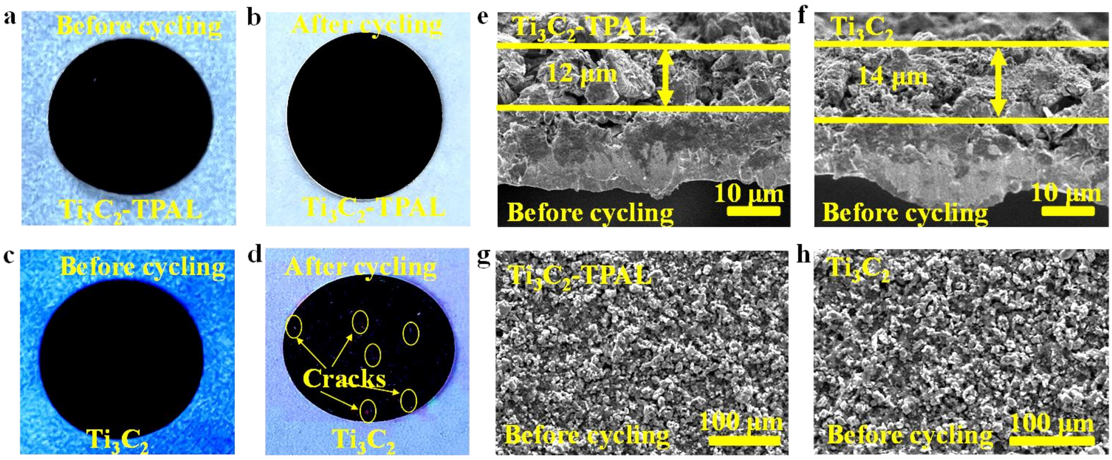

Supplementary Figure 13. Digital photographs of a, b) Ti_3C_2-TPAL and c, d) Ti_3C_2 before and after cycling. Cross-sectional SEM images of e) Ti_3C_2-TPAL and f) Ti_3C_2. Top-view SEM images of g) Ti_3C_2-TPAL and h) Ti_3C_2 (initial state).

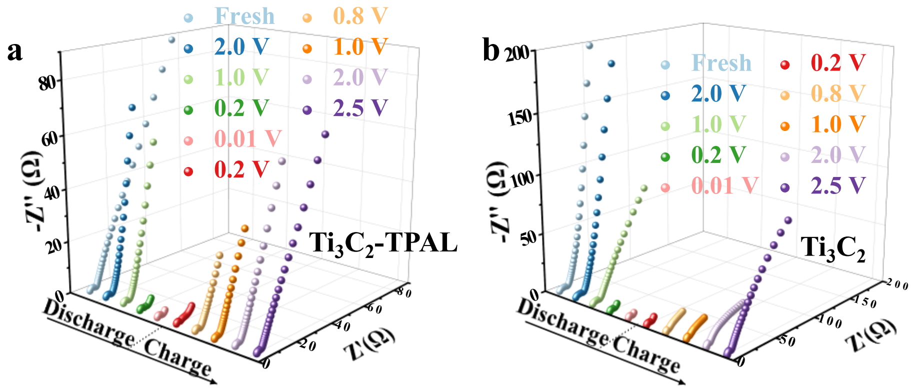

Supplementary Figure 14. Nyquist plots of a) Ti_3C_2-TPAL and b) Ti_3C_2 obtained during charging and discharging.

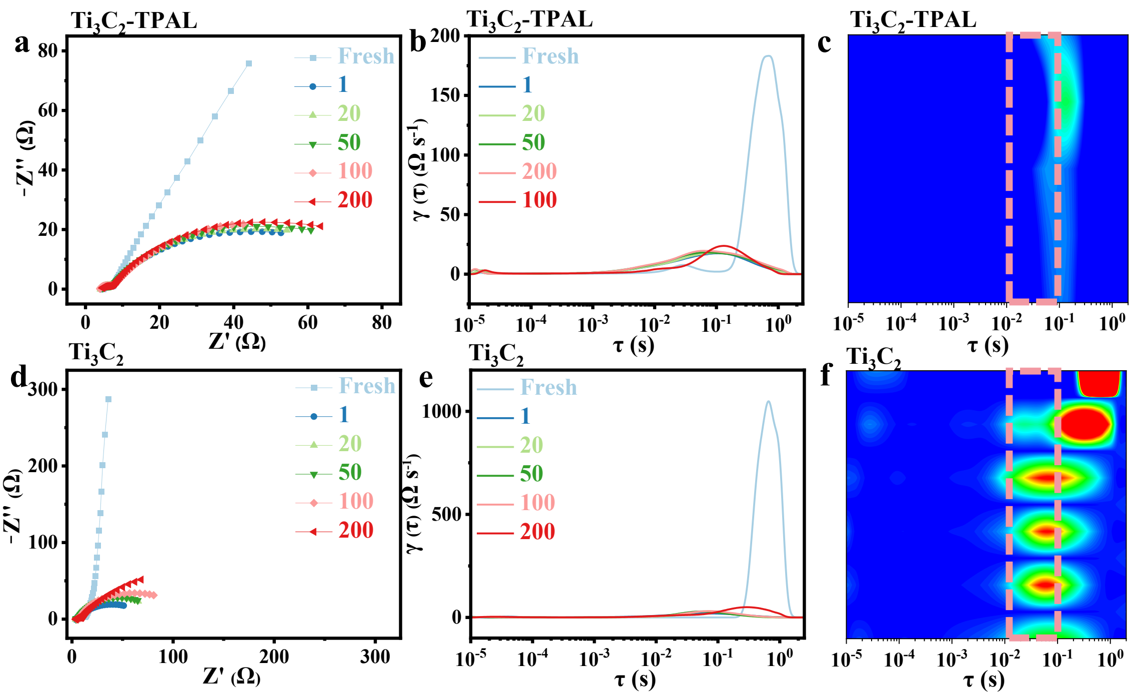

Supplementary Figure 15. EIS spectra, DRT plots, and intensity color maps of a-c) Ti_3C_2-TPAL and d-f) Ti_3C_2 collected at different cycle numbers.

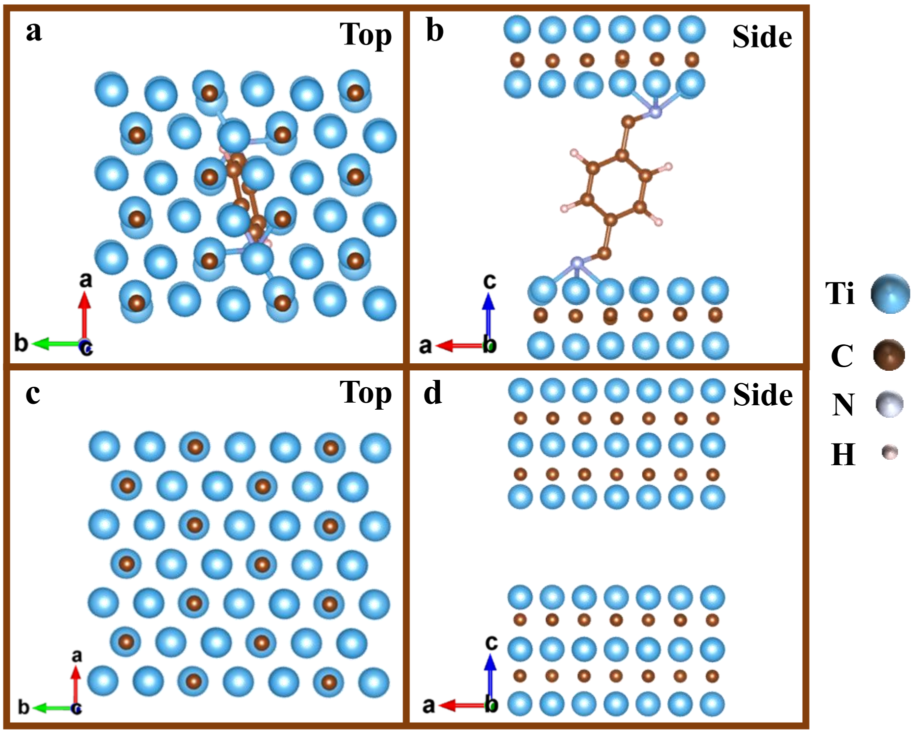

Supplementary Figure 16. Structural models for a, b) Ti_3C_2-TPAL and c, d) Ti_3C_2 calculated using DFT.

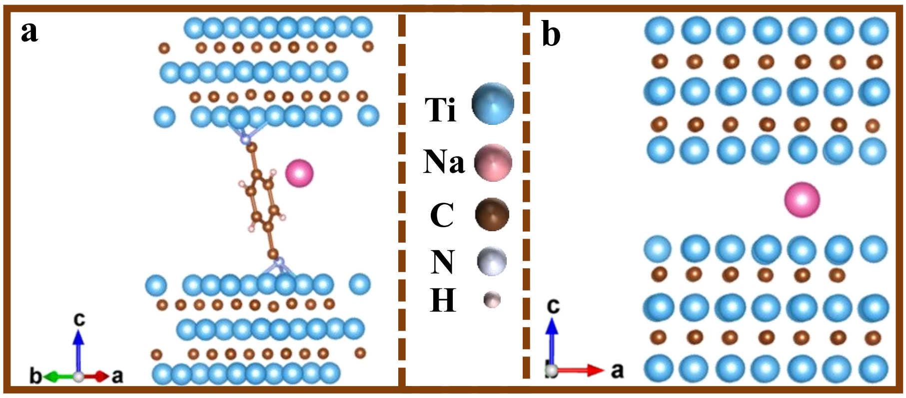

Supplementary Figure 17. DFT-optimized configurations of Na adsorbed on a) Ti_3C_2-TPAL and b) Ti_3C_2.

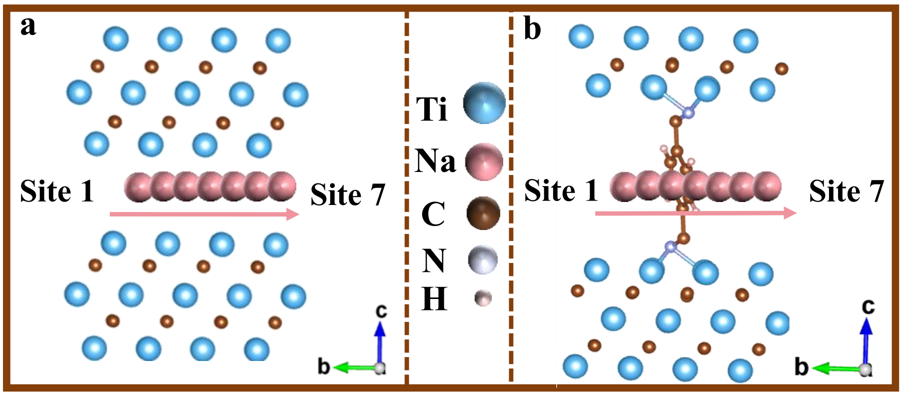

Supplementary Figure 18. Na^+ diffusion profiles in the interlayers of a) Ti_3C_2 and b) Ti_3C_2-TPAL.

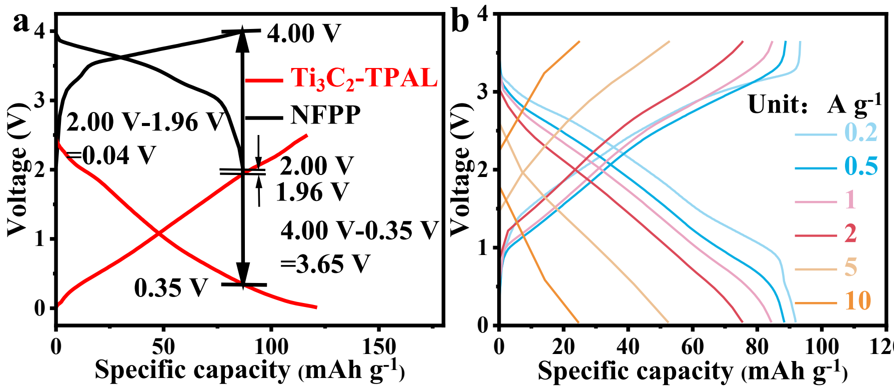

Supplementary Figure 19. a) GCD profiles of the Ti_3C_2-TPAL anode and NFPP cathode. b) Cycling performance of the Ti_3C_2-TPAL//NFPP full SIBs.

Supplementary Table 1. Comparison of the electrochemical performance of MXene-based anode materials for SIBs.

Samples	Specific capacity (mAh g^{-1})	Current density (A g^{-1})	Ref.
Ti_3C_2-TPAL	54.3 (after 2500 cycle)	5	This work
MXene	35 (after 100 cycle)	1	[S1]
as-$Ti_3C_2T_X$	45 (after 500 cycle)	0.1	[S2]
$Ti_3C_2T_X$	53 (after 1000 cycle)	5	[S3]
f-$Ti_3C_2T_X$_DMSO	75 (after 1500 cycle)	1	[S4]
$Na_{0.2}$-$Ti_3C_2T_X$	65 (after 100 cycle)	1	[S5]

Supplementary Table 2. Comparison of energy density and power density for MXene-based full SIBs.

Electrode materials	Energy density and power density	Ref.
Ti_3C_2-TPAL//NFPP	190.8 Wh kg^{-1} and 412 W kg^{-1} 155 Wh kg^{-1} and 876 W kg^{-1} 138 Wh kg^{-1} and 1644 W kg^{-1} 113 Wh kg^{-1} and 3019 W kg^{-1} 61 Wh kg^{-1} and 6099W kg^{-1} 18 Wh kg^{-1} and 9040 W kg^{-1}	This work
Na-Ti_3C_2//AC	80 Wh kg^{-1} and 250 W kg^{-1} 75 Wh kg^{-1} and 500 W kg^{-1} 65 Wh kg^{-1} and 1100 W kg^{-1} 60 Wh kg^{-1} and 2000 W kg^{-1} 45 Wh kg^{-1} and 4500 W kg^{-1}	[S6]
Bi-stacked MXene//AC	40 Wh kg^{-1} and 20 W kg^{-1} 38 Wh kg^{-1} and 45 W kg^{-1} 30 Wh kg^{-1} and 100 W kg^{-1} 28 Wh kg^{-1} and 200 W kg^{-1} 23 Wh kg^{-1} and 1140 W kg^{-1}	[S7]
$Ti_3C_2T_x$/Na_3-TCM//AC 1:3	70 Wh kg^{-1} and 2 W kg^{-1} 60 Wh kg^{-1} and 4 W kg^{-1} 48 Wh kg^{-1} and 6 W kg^{-1} 32 Wh kg^{-1} and 28 W kg^{-1} 18 Wh kg^{-1} and 50 W kg^{-1} 10 Wh kg^{-1} and 200 W kg^{-1}	[S8]
Ti_3CN–NH-SA//AC	80 Wh kg^{-1} and 200 W kg^{-1} 78 Wh kg^{-1} and 400 W kg^{-1} 70 Wh kg^{-1} and 1000 W kg^{-1} 60 Wh kg^{-1} and 2000 W kg^{-1} 50 Wh kg^{-1} and 4000 W kg^{-1}	[S9]
N-$Ti_3C_2T_x$//AC	100 Wh kg^{-1} and 60 W kg^{-1} 90 Wh kg^{-1} and 150W kg^{-1} 88 Wh kg^{-1} and 200 W kg^{-1} 80 Wh kg^{-1} and 600 W kg^{-1}	[S10]

References

S1. Xu, E.; Zhang, Y.; Wang, H.; et al. Ultrafast kinetics net electrode assembled via $MoSe_2$/MXene heterojunction for high-performance sodium-ion batteries. *Chem. Eng. J.* **2020**, *385*, 123839. DOI: 10.1016/j.cej.2019.123839.

S2. Lv, G.; Wang, J.; Shi, Z.; et al. Intercalation and delamination of two-dimensional MXene ($Ti_3C_2T_x$) and application in sodium-ion batteries. *Mater. Lett*. **2018**, *219*, 45-50. DOI: 10.1016/j.matlet.2018.02.016.

S3. Fan, Z.; Wei, C.; Yu, L.; et al. 3D Printing of Porous Nitrogen-Doped Ti_3C_2 MXene Scaffolds for High-

Performance Sodium-Ion Hybrid Capacitors. *ACS Nano*. **2020**, *14*, 867-76. DOI: 10.1021/acsnano.9b08030.

S4. Wu, Y.; Nie, P.; Wang, J.; et al. Few-Layer MXenes Delaminated via High-Energy Mechanical Milling for Enhanced Sodium-Ion Batteries Performance. *ACS AMI*. **2017**, *9*, 39610-7. DOI: 10.1021/acsami.7b12155.

S5. Brady, A.; Liang, K.; Vuong, V.Q.; et al. Pre-Sodiated $Ti_3C_2T_x$ MXene Structure and Behavior as Electrode for Sodium-Ion Capacitors. *ACS Nano*. **2021**, *15*, 2994-3003. DOI: 10.1021/acsnano.0c09301.

S6. Luo, J.; Fang, C.; Jin, C.; et al. Tunable pseudocapacitance storage of MXene by cation pillaring for high performance sodium-ion capacitors. *J. Mater. Chem. A*. **2018**, *6*, 7794-806. DOI: 10.1039/C8TA02068J.

S7. Kurra, N.; Alhabeb, M.; Maleski, K.; et al. Bistacked Titanium Carbide (MXene) Anodes for Hybrid Sodium-Ion Capacitors. *ACS Energy Lett*. **2018**, *3*, 2094-100. DOI: 10.1021/acsenergylett.8b01062.

S8. Liu, S.; Hu, F.; Shao, W.; et al. A Novel Strategy of In Situ Trimerization of Cyano Groups Between the $Ti_3C_2T_x$ (MXene) Interlayers for High-Energy and High-Power Sodium-Ion Capacitors. *Nano-Micro Lett*. **2020**, *12*, 135. DOI: 10.1007/s40820-020-00473-7.

S9. Zhang, J.; Zhang, D. Organic-inorganic coupled Ti_3CN MXene achieving the excellent sodium-ion storage performance. *Electrochimica. Acta*. **2024**, *507*, 145102. DOI: 10.1016/j.electacta.2024.145102.

S10. Yuan, J.; Pan, D.; Chen, J.; et al. Ultrafast Na-Ion Storage in Amorphization Engineered Hollow Vanadium Oxide/MXene Nanohybrids for High-Performance Sodium-Ion Hybrid Capacitors. *Adv. Mater*. **2024**, *36*, 2408923. DOI: 10.1002/adma.202408923.